Analytical and Numerical Model Analysis of Elastocaloric Cooling Systems

K. Madhusudhana Reddy[1], K. Prahlada Rao[2]
[1]M.Tech student, Mechanical Engineering, JNTUA College Of Engineering, Anantapuramu, India.
[2]Professor, Mechanical Engineering, JNTUA College of Engineering, Anantapuramu, India.

ABSTRACT : Vapour compression (VC) is by far the most dominant technology for meeting all cooling and refrigeration needs around the world. It is a mature technology with the efficiency of modern compressors approaching the theoretical limit, but its environmental foot prints remains a global problem as VC cooling refrigerants are considered to have high global warming potential (GWP). As an alternate option other than using low GWP refrigerants and natural refrigerants, Solid-state cooling technologies show their advantage of zero GWP. Elastocaloric cooling technology uses shape memory alloys (SMA), these are a group of metal alloys with significant elastocaloric effect. They can be used for power cycles, or applied reversely for themoelastic cooling/heat pump cycles. Elastocaloric (Thermoelastic) cooling shows better thermal potential compared with other Solid-state cooling technologies such as Thermoelectric cooling, Thermoacoustic cooling and Magnetic cooling. In this dissertation work Elastocaloric single-stage cooling cycle design options are introduced first. Then analytical coefficient of performance equation is derived for reverse Brayton cycle design. Effects of heat transfer Effectiveness, heat recovery Efficiency and Temperature lift on system COP are investigated under constant cycle duration. A Numerical model is developed to evaluate the Brayton cycle (used NiTi alloy tube as the material for SMA beds) performance under cyclic operation mode. Simple parametric study is conducted to study the role of various operating parameters such as cycle duration, Heat transfer velocity , Heat recovery velocity and geometric parameter such as Wall thickness on system COP and Cooling capacity using MATLAB .

Keywords : **Nitinol, Solid-state cooling, Shape memory alloy, Elastocaloric cooling systems**

I. INTRODUCTION

Recently, traditional refrigerants in a vapour compression system, such as hydrochloroflurocarbons (HCFs) and Hydrofluo rocarbons (HFCs), have been considered as green house gases exaggerating the global warming crisis. Most of the HFCs have high global warming potential (GWP), each of which molecule is equivalent to more than 1,000 CO2 molecules (EPA database, 2014). Solid-state cooling systems offer us alternative to eliminate the emission of traditional high global warming potential (GWP) halogenated refrigerants used in the vapour compression cycle (VCC) systems. Elastocaloric effect has a higher adiabatic temperature span as well as thermoelastic materials have better material level performance compared to other solid-state cooling technologies such as Thermoelectric, Thermoacoustic and Magnetocaloric cooling (Qian et al., 2015)[1]. Elasocaloric cooling technology uses shape memory alloys (SMA), which is a group of metal alloys with significant elastocaloric effect. They can be used for power cycle or applied reversely for thermoelastic cooling/heat pump cycles. Required cooling/heating effect in cooling/heat pump is the result of the associated latent heat released during the stress induced martensitic phase change process, which makes the material transits between martensite phase and austenite phase.

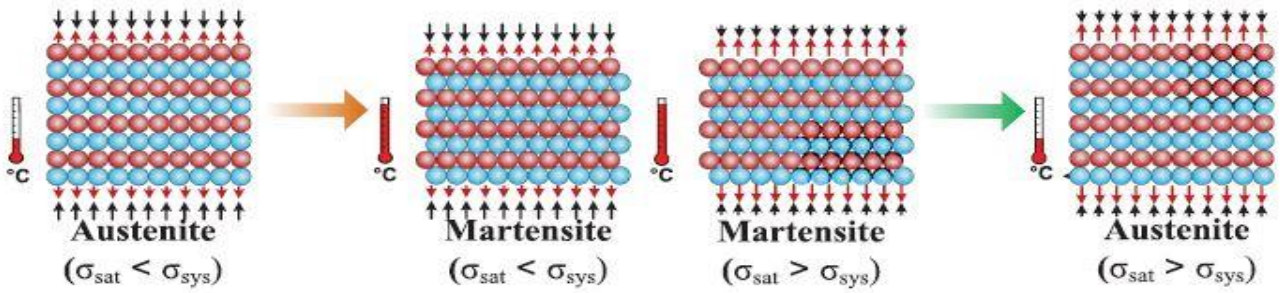

a) Stress induced phase change releasing latent heat and (σsat < σsys)

b) Releasing stress leads to reversed phase change and absorbing latent heat (σsat > σsys)

Fig .1 -- Illustration of martensite phase change process.

As show in Fig.1(a), when the SMA is subjected to an external stress exceeding the phase change stress σsat . When the stress decreases below the threshold, the material transits back to the austenite state and absorbs surroundings heat. Shape

memory alloys have peculiar mechanical property that it "remembers" an original" trained" shape, and can return to this pre-deformed shape upon heating above a transitional temperature.

There are two main concerns considered in this study to distinguish this from previous literature. First one is decoupling of stress strain relation from temperature to avoid complexity in calculation of the work needed to drive the cooling/heat pump cycle ,experimental data were used to fit in a simple one-dimensional constitutive model, in order to evaluate the loading/unloading energy related to the coefficient of performance (COP) for this study. Second one is consideration of heat recovery/regeneration process to improve the efficiency and heat transfer fluid loops and associated losses in analysis. Apart from the above two concerns The field of using SMA for cooling/heat pump cycle is completely new, and therefore a guideline on thermodynamic cycle analysis and modelling is necessary.

II. LITERARTURE REVIEW

A comprehensive review of shape memory materials, including SMAs, shape memory ceramics and SMPs, was carried out by Otsuka and Wayman (1998)[2]. The Ni base alloys, especially Ni-Ti alloy, had become the most popular SMA and dominated the market after its discovery in 1959 (Buehler et al., 1963)[3] from Naval Ordanance Laboratory, where the Ni-Ti was named for nitinol since then. Cu-based family of SMAs were also popular, since Cu is much cheaper than Ti. Binary alloy including Cu-Zn (Romero and Pelegrina, 2003)[4] and Cu-Sn (Miura et al., 1975)[5] were investigated in literature. Banks (1975)[6] invented the first continuously opearating SMA heat engine. Johnson (1979)[7] improved Banks design by adding the regeneration process and changed the layout accordingly.. Brayton cycle, with COP of 6 operated under 17 K temperature lift was mentioned in the report, believed to be simulated by Elastek's model. Hugenroth (2002)[8] patented the two pulleys design for SMAs operated under Brayton cycle, but unfortunately no heat recovery/regeneration was implemented. Cui et al. (2012)[9] patented various driving mechanisms with heat recovery/regeneration, for both compression and tension options. Thermoelastic cooling systems cycle options, thermodynamic analysis, and dynamic modeling were presented by S.Qian, JLing, Y.Hwang ,R.Radermacher, Takeuchi[10].

In this dissertation work Elastocaloric single-stage cooling cycle design options are introduced first. Then analytical coefficient of performance equation is presented for reverse Brayton cycle design. Effects of heat transfer Effectiveness, heat recovery Efficiency and Temperature lift on system COP are investigated under constant cycle duration. A Numerical model is developed to evaluate the Brayton cycle (used NiTi alloy tube as the material for SMA beds) performance under cyclic operation mode. Simple parametric study is conducted to study the role of various operating parameters such as cycle duration, Heat transfer velocity , Heat recovery velocity and geometric parameter such as Wall thickness on system COP and Cooling capacity using MATLAB.

III. BASIC THERMODYNAMIC CYCLES OF ELASTOCALORIC COOLING SYSTEMS

Thermoelastic cooling/heat pump cycle can be achieved via two two basic thermodynamic cycles: i) Reverse Brayton cycle in Fig. 3 and ii) Reverse Stirling cycle in Fig. 4

i) Reverse Brayton cycle:

The reverse Brayton cycle consists of two isentropic processes and two iso-stress processes. The material is under unstressed austenite phase at state 1 and then stress is loaded to the material causing it moves to state 1' and martensitic phase change starts. The associated latent heat is then released from 1' to 2 adiabatically, causing the temperature to increase on the T-S diagram. Then heat transfer takes place and the SMA temperature approaches heat sink's temperature at Th, while the material itself is still fully stressed at martensite phase. Before fully unstressed, the SMA can be further cooled down to 4 by exchanging the sensible heat between one set of SMA material starting at state 3, and another set of SMA material just finished cooling the conditioned space at state 6. The heat exchange process is so called a heat recovery process. Thermodynamics allows a 100% heat recovery efficiency, which means state 4 temperature could be the same as state 6 temperature. A reverse adiabatic phase change process brings the SMA back to austenite from 4' to 5. This process is called unloading . During the rest of the cycle, the SMA remains unstressed. The cooling process to the conditioned space is from 5 to 6, and reverse heat recovery process is from 6 back to 1 with the other set of SMA materials undergoes the process from 3 to 4. The heat recovery process conserves energy, and therefore the heat rejected to the sink should be equal to the summation of the heat absorbed from the conditioned space and the work needed to drive one cycle. It should be noted that the area underneath 1–1'–2 on the σ–e (stress–strain) diagram is the loading work, and the area underneath 4–4'–1 is the unloading work. If the system is designed properly, the unloading work can be fully used to compensate part of the loading work. Therefore, the area surrounding by the cycle on σ–e diagram is corresponding to the net power input with 100% work recovery design.

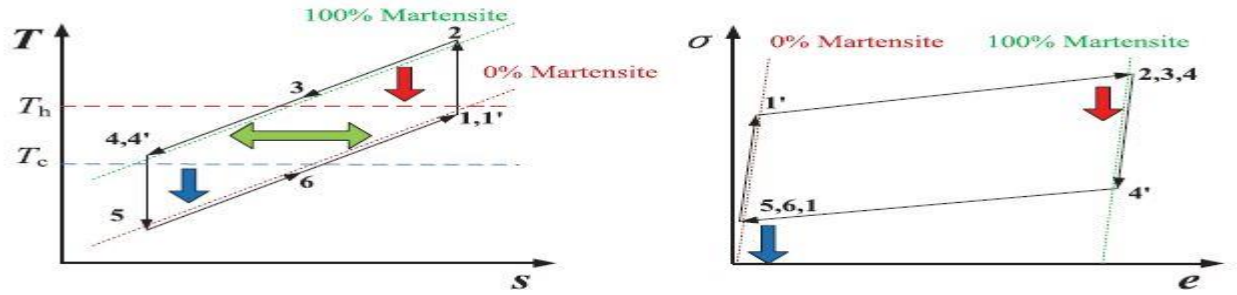

Fig.2 Illustration of reverse Brayton cycle and its variation as a thermoelastic cooling cycle

ii) Reverse Stirling cycle:

Reverse stirling cycle contains two iso-stress heat transfer processes, and two isothermal phase change processes. The cycle begins at unstressed state 1, and is stressed to 1' before the phase change begins. Different from reverse Brayton cycle, the SMA material is cooled during the martensitic phase transformation process from 1' to 2', and therefore keeps a constant temperature while releasing the latent heat. The iso-stress heat recovery process from 2 to 3 is essentially the same as previously introduced. Afterwards, the unloading process from 3 to 4 via 3' takes place with the isothermal heating process, where the conditioned room air is cooled down by the system . The cycle concludes by the iso- stress heat recovery process.

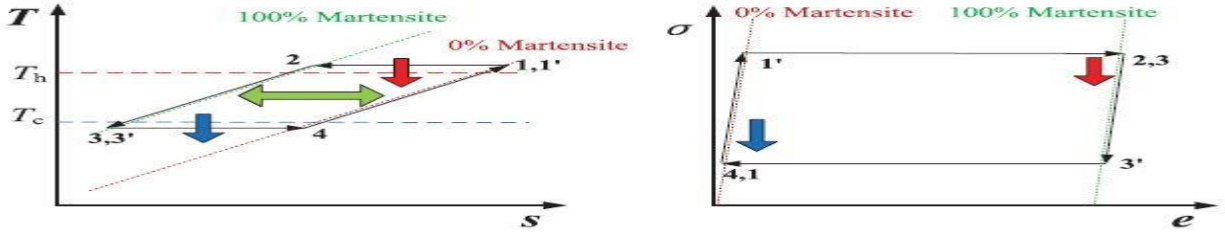

Fig. 3 Illustration of reverse Stirling cycle and its variation as a thermoelastic cooling cycle.

IV. ANALYTICAL MODEL OF ELASTOCALORIC COOLING

In this work, Reverse Brayton cycle design is considered for analysis, as shown in Fig. 3. For a reverse Brayton cycle design with two beds, the time scale of phase change is much smaller that that of the heat transfer.

The derivation of the analytical COP and cooling capacity requires physical understanding of the solid –state material temperature change during a single cooling cycle.

Assumptions:

- Lump temperature for solid-state materials
- Same heat transfer effectiveness for both solid-state materials during both cooling and heating process
- Same cooling and heating heat recovery efficiency
- Same adiabatic temperature span for stress induced phase change (the phase change from martensite to austentite has the same temperature span as the one from the austenite to martensite)

For adiabatic phase change process

$$T_2 - T_1 = T_4 - T_5 = \Delta T_{ad} \qquad (1)$$

For solid-state material, heat transfer processes (2→3 and 5→6)

$$\frac{T2-T3}{T2-Th} = \frac{T6-T5}{Tc-T5} = \varepsilon \qquad (2)$$

For heat recovery processes (3→4 and 6→1')

$$\frac{T3-T4}{T3-T6} = \frac{T1\prime-T6}{T3-T6} = \eta_{HR} = \eta \qquad (3)$$

The material cooling capacity could be evaluated by

$$Q_{mat} = \frac{mcp}{tcyc}(T_6\text{-}T_5) \qquad (4)$$

Where m is the total mass of solid-state material in a single bed, and t_{cyc} is the cycle duration. When considering the entire cooling system, the fluid cooling capacity deviates from the material cooling capacity. This is because part of the cooling power released from the solid-state material is lost along the pipe to the heat exchanger due to fluid mixing. Heat loss to ambient, and temperature cycling. Such difference caused by irreversibility could be measured by a factor F less than 1. On the other hand, the real power consumption to drive the solid state material loading–unloading process also

deviates from the theoretical value. This difference is due to motor efficiency η_{mot} , transmission efficiency η_{trsm} , and work-recovery efficiency η_{rec} . A similar factor could be applied to evaluate this deviation with the factor D

$$F = \frac{Qfluid}{Qmat} \quad (5) \qquad D = \frac{Wideal}{Wreal} = \eta_{mot}\eta_{trsm}\frac{w+ - w-}{w+ - \eta recw-} \quad (6)$$

In the context of vapour compression heat pump, this factor D is similar to the compressor efficiency. Work recovery is similar to a turbine, where part of the available energy from the high pressure refrigerant is re-used to reduce compressor work.

$$\frac{Qmat}{Qlat} = \frac{T6-T5}{T2-T1} \quad (7) \qquad \Delta T_{lift} = T_h - T_c \quad (8)$$

The system COP is defined as the ratio between gain and cost:

$$COP = \frac{Qfluid}{Wreal} = \frac{Qfluid}{Qmat}.\frac{Qmat}{Qlatent}.\frac{Qlatent}{Wideal}.\frac{Wideal}{Wreal} = F.\frac{Qmat}{Q\ latent}.COP_{mat}.D \quad (9)$$

The second term could be evaluated from Eqs. 1–4:

$$\frac{Qmat}{Qlatent} = \frac{\varepsilon\,(\Delta Tad - \Delta Tlift(1-\eta))}{\Delta Tad[1+(1-\varepsilon)(1-2\eta)]} = \frac{\varepsilon(\gamma+\eta-1)}{\gamma[1+(1-\varepsilon)(1-2\eta)]} \quad (10)$$

The system COP and cooling capacity are:

$$COP = F\ \frac{\varepsilon(\gamma+\eta-1)}{\gamma[1+(1-\varepsilon)(1-2\eta)]}.D.\ COP_{mat} \quad (11)$$

$$Q_{fluid} = F.\frac{mcp\Delta Tlift}{tcyc}.\frac{\varepsilon(\gamma+\eta-1)}{\gamma[1+(1-\varepsilon)(1-2\eta)]} \quad (12)$$

V NUMERICAL MODEL OF ELASTOCALORIC COOLING SYSTEMS

In the numerical dynamic model, the following assumptions are used:

- The timescales of phase transformation and loading are negligible compared with that of heat transfer
- Radial heat transfer time scale is negligible compared with axial direction Bi = 0.01
- Uniaxial loading and uniform phase transformation
- Constant thermophysical properties with the small temperature of interest
- Incompressible flow and uniform velocity profile at any cross section inside the nitinol tube
- No heat transfer from nitinol tubes to surroundings
- No radiation heat transfer

It should be noted that the first assumption is crucial to the dynamic model simulation, because it not only decouples the problem , but also transforms a stiff problem to a normal problem and therefore, improve the robustness of the simulation.The adiabatic phase transformation process as 1→ 2or 4→ 5 in Fig2, is completed within 0.1s, which is two magnitudes less than the heat transfer/heat recovery time scale.

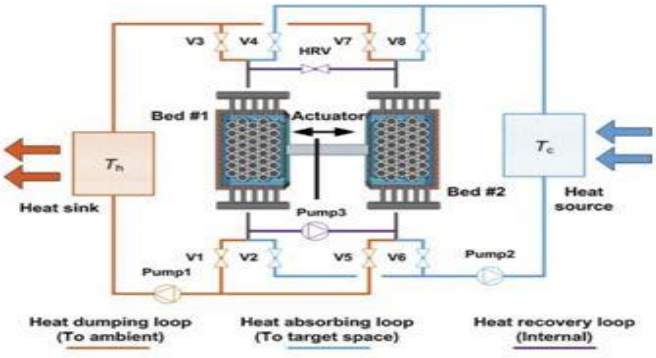

Fig.4 Schematic of the heat transfer fluid loop used for model

Process	1→1'→2	2→3	3→4	4→4'→5	5→6	6→1'
Description	Adiabatic phase change	Heat transfer	Heat recovery	Adiabatic phase change	Heat transfer	Heat recovery
V1	X	O	X	X	X	X
V2	X	X	X	X	O	X
V3	X	O	X	X	X	X
V4	X	X	X	X	O	X
V5	X	X	X	X	O	X
V6	X	O	X	X	X	X
V7	X	X	X	X	O	X
V8	X	O	X	X	X	X
HRV	X	X	O	X	X	O
Pump1	X	O	X	X	O	X
Pump2	X	O	X	X	O	X
Pump3	X	X	O	X	X	O
$\dot{g}$	1/τ-	0	0	1/τ-	0	0

Note: "X" is close/off, "O" is open/on.

Table2:Valves and pump sequences of model

Fig. 4 shows the schematic of the thermoelastic cooling system model. There are four basic components in the the model: thermoelastic material beds, heat source/sink, mechanical driver, and connecting pipes (three colours representing different loops). The two beds design enables heat recovery, work recovery of the mechanical driver and the continuous cooling/heating production. The mechanical driving system can by any linear actuator, i.e. linear screw jack driven by motors, or hydraulic cylinder driven by oil pump, which can move reciprocally to compress each bed one by one. When one bed is compressed, the other bed is unloaded. During the loading process, the work recovery requires the unloading energy from the other bed to be applied in order to save the power consumption of the driving system. Referring to Fig. 2 for SMA beds temperature change, the mechanical driving system and the HTF loops must operate and synchronize in a certain order to guarantee proper cycle operation as specified in table2.

Table 1 – Physical properties and phase change parameters of some common SMA with giant elastocaloric effect. ([a]).

Materials	NiTi	CuZnAl	CuAlNi
Density [kg m^{-3}]	6400–6500 (6500)	7500–8000 (7900)	7100–7200 (7150)
c_p [J kg^{-1} K^{-1}]	470–620 (550)	390–400 (400)	373–480 (440)
Conductivity [W m^{-1} K^{-1}]	8.6–18 (18)	84–120 (120)	30–75 (75)
Δs [J kg^{-1} K^{-1}]	42	19–26 (20)	20–30 (20)
ΔT_{ad} [K]	22.9 (300 K)	15.0 (300 K)	13.6 (300 K)
Transformation temperature [°C]	−200–200	−200–150	−200–200
A [J kg^{-1}]	120	155	280
K [MPa]	1.72×10^4	3.10×10^4	4.90×10^3
Δ	0.02	0.025	0.029
$w+$ (Brayton) [J g^{-1}]	5.64	1.58	3.02
$w-$ (Brayton) [J g^{-1}]	4.14	0.78	1.99
w_{net} (Brayton) [J g^{-1}]	1.50	0.80	1.03
γ	2.29	1.50	1.36
COP_{mat} (Brayton)	2.5 (Tensile)	6.9 (Tensile)	7.6 (Tensile)
	8.0 (Compressive)	6.8 (Compressive)	5.2 (Compressive)
COP_{mat} (Stirling)	3.4 (Tensile)	11.9 (Tensile)	11.9 (Tensile)
	15.5 (Compressive)	11.4 (Compressive)	7.2 (Compressive)
Data reference	Cui et al., 2012	Ziolkowski, 1993	Friend and Hamilton, 1995
	Smith et al., 1993	Otsuka and Wayman, 1998	Rodriguez and Brown, 1980
	Otsuka and Wayman, 1998	Bonnot et al., 2008	Huang, 2002
		Manosa et al., 1993	Chen et al., 2009
		Manosa et al., 2009	Picornell et al., 2001
		Sittner and Novak, 2000	Picornell et al., 2004
		Manosa et al., 2013	
		Gall et al., 1998	
		Lashley et al., 2007	

NiTi: Ni 55 wt%; CuZnAl: Cu 65 wt% – 70 wt%, Al 13 wt% – 23 wt%; CuAlNi: Al 12–15 wt%, Cu 80 wt% – 85 wt%.
Also, 288 K–298 K heat pump with 10 K temperature lift is used to evaluate the non-dimensional latent heat γ and other temperature dependent parameters here in this table.
[a] The numbers in bracket are specific numbers used for all calculation in this study.

The governing equations of thermoelastic material beds are energy equations for solid tube and fluid inside, as shown in Eqs. 13 and 14.

$$\frac{\partial Ts}{\partial t} = \alpha_s \frac{\partial^2 Ts}{\partial x^2} - \frac{h}{\delta.(\rho Cp)s}(T_s - T_f) + \frac{g''}{(\rho Cp)s} \quad (13)$$

$$\frac{\partial Tf}{\partial t} = \alpha_f \frac{\partial^2 Tf}{\partial x^2} - \frac{4h}{ID.(\rho Cp)f}(T_f - T_s) - u_f \frac{\partial Tf}{\partial x} \quad (14)$$

For solid energy equation Eq. 13, the first term on the RHS identifies the conduction along axial direction (flow direction), and the second term measures the convective heat transfer between solid and fluid contact with solid. Most importantly, the last term is determined by the thermoelastic effect, which is positive during the austenite to martensite transformation process and negative during the opposite process. The term remains zero when there is no phase transformation. Assuming that loading/unloading processes and the latent heat are independent on temperatures, this simplification makes sense since the time scale for phase change(~0.1s) is much smaller than the time scale for heat transfer (~ 1-10 s). Despite an ideal scenario that stress-strain relation could be decoupled from temperature, Such decoupling leads to a much easier calculation of the generation term, as indicated by Eq. (15)

$$\text{.g"} = \begin{cases} \rho(\Delta h + W +) \frac{de}{emaxdt} = \rho(\Delta h + W +) \tilde{e} \;\; \tilde{e} = € \geq 0 \\ \rho(\Delta h + W +) \frac{de}{emaxdt} = \rho(\Delta h + W +) \tilde{e} \;\; \tilde{e} = € < 0 \end{cases} \quad (15)$$

In Eq. (15), the loading process releases heat, therefore generation term is greater than zero. Both latent heat released from the phase change process Δh and mechanical stress induced deformation energy w+ are accounted, vice versa. It also holds for single phase heat transfer and heat recovery process, since the time derivative of normalized strain is zero when no phase change occurs. Here since we assume uniform phase change, the martensite phase fraction rate is same as deformation strain rate. The strain profile is determined in Table 2.

$$\frac{\partial Ts}{\partial x}|x = 0, x = L = 0 \quad (16) \qquad T_f|x = 0 = T_{f,in} \quad (17)$$

Adiabatic boundary conditions are applied for solid in Eq (16) and commonly used boundary conditions for fluid are set in Eq. (17

$$m_c c_{p,f} \frac{dTc}{dt} = \dot{m}_c c_{p,f} (T_{in} - T_c) + \dot{Q}_c \quad (18)$$

A uniform temperature water tank model is applied for both heat source /sink, as shown in Eq. (18). The heat source is assumed to have a heat rate of $\dot{Q}_c$, which is determined by a PID controller using T_c and $T_{c,set}$ as control signals. The set points for heat source T_c and T_h are determined based on temperature lift.

$$\frac{\partial Tf}{\partial t} = \frac{kf}{k(\rho Cp)f} \frac{\partial 2Tf}{\partial x2} - \frac{4hair}{k.(\rho Cp)fOD} (T_f - T_{amb}) - \frac{uf}{k} \frac{\partial Tf}{\partial x} \quad (19)$$

$$k = \frac{(mCp)f+(mCp)s}{(mCp)f} = \frac{(\rho Cp)fID^2+(\rho Cp)s\,(OD^2-ID^2)}{(\rho Cp)fID^2} \quad (20)$$

For the connecting pipes, only fluid energy equation is used, with a correcting factor k to account for the thermal mass contribution from solid pipe wall, as shown in Eqs. 19 and 20

The valve/pump sequences specified in Table 2 are used to determine the flow rate and corresponding velocity for each pipe in Fig. 4. When the valves are closed, it is assumed that the flow stops instantaneously without any delay, and vice versa. Water is used as the heat transfer fluid for all fluid loops. The following correlations are currently used to pipe flow heat transfer coefficient h, for both regular pipes and thermoelastic material tubes.

Laminar flow : $Nu_D = 3.66$ (fully developed constant wall temperature).

Turbulent flow : $Nu_D = 0.023 Re_D^{(4/5)} Pr^n$ (Dittus-Boelter equation).

Similar to other cyclic operated cooling systems such adsorption chiller, the thermoelastic cooling system instantaneous cooling capacity, or the RHS second term in Eq. 17, is also varying all the time. Instead, the time averaged cooling capacity $\overline{Qc}$ during the cyclic steady state condition is used, and COP is also evaluated based on the time averaged capacity, as shown in Eqs. 21 and 22

$$\overline{Qc} = \frac{\int_0^{tcyc} \dot{Q}c\,dt}{tcyc} \quad (21$$

$$COP = \frac{\overline{\dot{Q}c}\,tcyc}{ms(W+ - \eta recW-)} \eta_{mot}\,\eta trms \quad (22)$$

In this study, it is assumed that $\eta_{mot}\,\eta trms = 0.9$, and work recovery efficiency $\eta_{rec} = 0.9$. To quantitatively study the thermoelastic cooling system performance, and investigate the most favorable material from a thermodynamic system perspective, necessary physical properties and loading test data are summarized in Table.1

VI RESULTS AND DISCUSSION

A) Variation of Analytical COP:

The sensitivity analysis of heat recovery efficiency, heat transfer effectivenss and temperature lift on COP is shown in Fig 5-7.The non dimensional latent heat (ɣ) evaluated at 10 K is available in Table 1.

Fig. 5 shows the effect of heat recovery efficiency on system COP when the cycle duration remains constant. The maximum COP improvements for all three alloys are all beyond 100% between the worst case scenario (η = 0.3) and the ideal case (η=1). Even when the heat recovery efficiency is 0.7, the improvement is more than 50% compared with the

worst case scenario. It should be noted that the heat recovery process favors more to those materials with higher specific heat, since the process saves more internal parasitic sensible heat for higher specific heat materials.

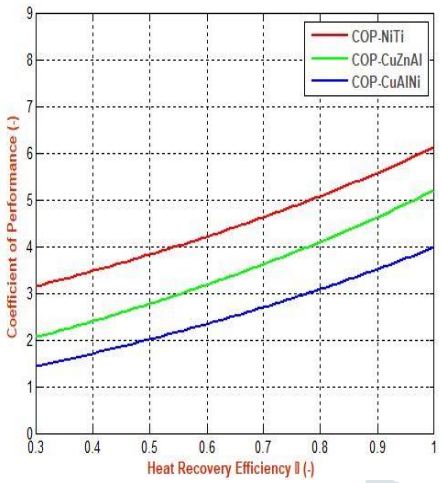

Fig 5: COP vs η
(F=0.9,ΔTlift=10 K, ε= 0.8, D=0.85

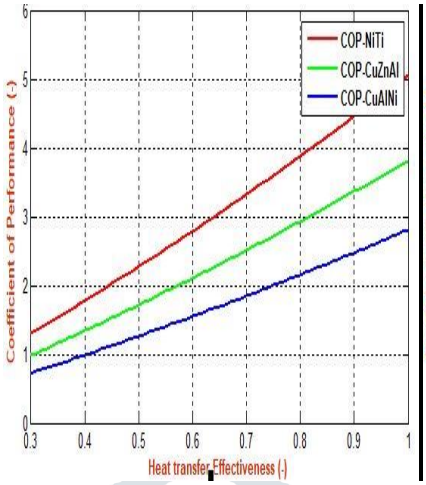

Fig 6: COP vs ε
(F=0.9,ΔTlift=10 K, η= 0.6, D=0.85)

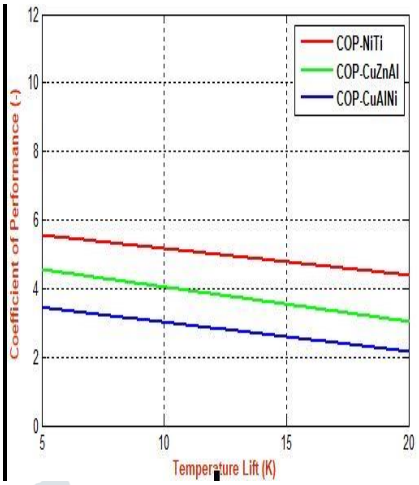

Fig 7: COP vs ΔT_{lift}
(F=0.9,ΔTlift=10 K, ε= 0.95,η=0.7 D=0.85)

Fig. 6 indicates that any insufficient heat transfer (processes 2→3, 5→6 in Fig.5) will lead to significant performance deterioration. For normal operation conditions, the effectiveness is usually greater than 0.8. The COP improvement is from 0.8 to 1 is 19%, which is not much significant as heat recovery efficiency, the COP improvement by heat transfer effectiveness is independent of SMA properties.

Fig. 7 plots how fast the performance reduces with respect to temperature lift and indicates a concave decreasing trend. Maximum temperature lift is achieved when there is no cooling or heating load, i.e. COP=0 since there is no cooling benefit. Under the extreme case when the heat recovery efficiency becomes 100%, there is no more limit on the maximum system temperature lift, and COP becomes independent on temperature lift as well. As heat recovery efficiency to be 100%, the bed 1 and bed 2 simply swap their temperatures from 3→4 and 6→1', which is not effected by how far away the heat source/sink lines are away.

B) Temperature Profiles of NiTi beds:

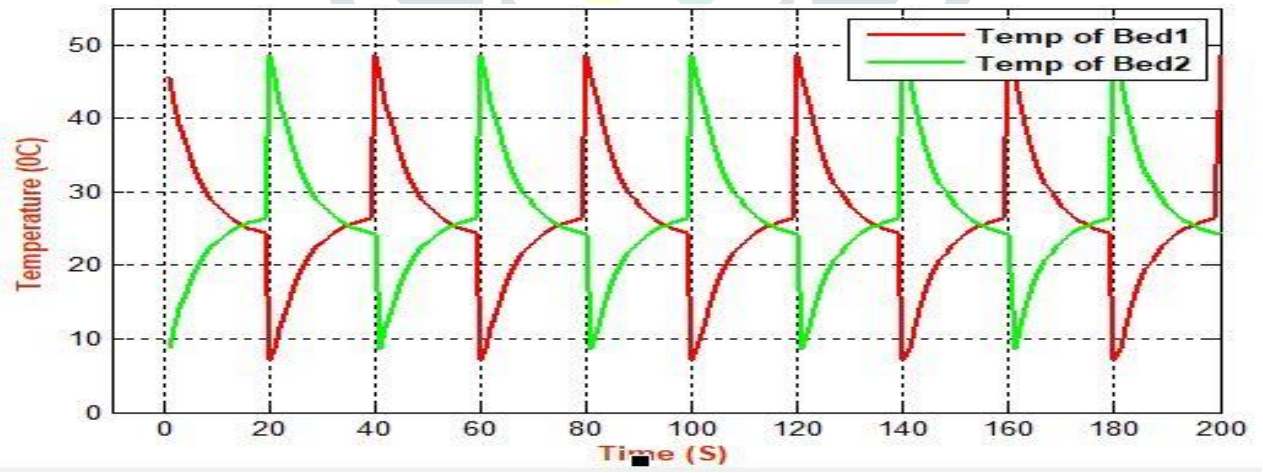

Fig 8:Temperature profiles predicted by the numerical model (NiTi alloy, uHT = 1.2 m/s, uHR =0.1m/ s, L=0.254 m, OD=0.005 m, ID= 0.004 m, N =19, ΔTlift=10 K, half cycle duration tcyc= 20 s)

Fig. 8 plots the temperature profiles of two NiTi beds for five complete cooling cycles under the "cyclic steady state" condition. Cyclic steady state refers to the period that the any measured variables repeat the same pattern over cycles, such as temperature profiles at a certain location all numerical model results used for discussion in this paper is sampled under such "cyclic steady state" condition. Note that the temperature variation is due to the cyclic operation nature of the system,

since cooling and heating are only provided during heat transfer process. The temperature lift determines the set points for heat source and heat sink.

C) Effect of Operating Parameters On System Performance

i) Effect of Half cycle duration on system COP and Cooling capacity:

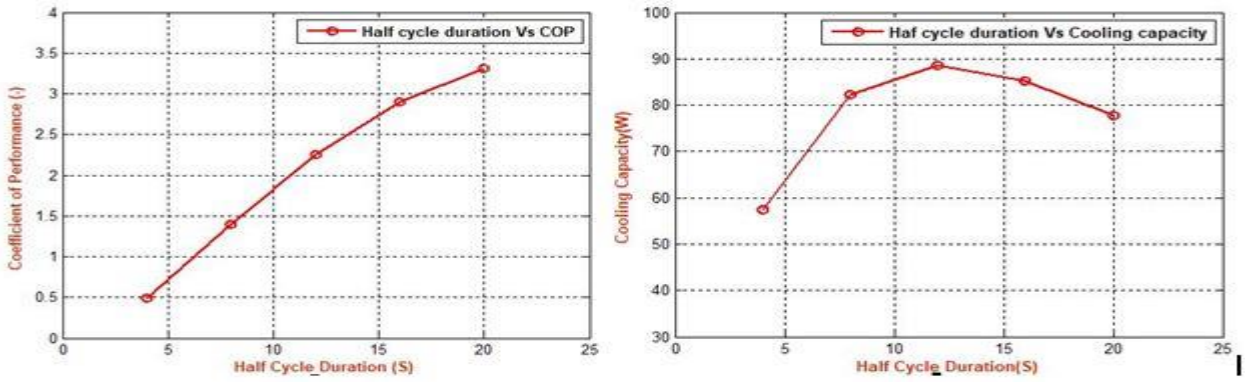

Fig 9:COP and cooling capacity as a function of cycle duration (Ni-Ti alloy, uHT = 1.2 m/s, L = 0.254 m, OD = 0.005 m, ID = 0.004 m, N = 19, ΔTlift = 10 K).

Half cycle duration is the most significant contributing factor to the system performance. Higher cycle duration has a more "complete" heat transfer and a more reversible heat recovery, therefore both heat transfer effectiveness(ε) and heat recovery efficiency (η) increases. As indicated by Eq. (10), the COP increases with a higher ε and η. From the figure it is evident that COP increases steadily but the rate of improvement is higher when cycle duration changed from 6s to 10s(COP from 0.65 to 1.75 -169%) compared to change of cycle duration from 10s to 20s (COP from 1.75 to 3.2(82%),. Meanwhile, the work per cycle remains the same. Here it is observed that time averaged cooling capacity increases upto certain cycle duration then decreases. The reason for this is increase in cycle duration is more in comparison with increase in cooling capacity. As a result time averaged cooling capacity decreases. Therefore while considering optimum cycle duration trade off should be made between improvement in COP and and decrease in Cooling capcity.

ii) Effect of Heat transfer velocity u_{HT} on system COP and Cooling capacity:.

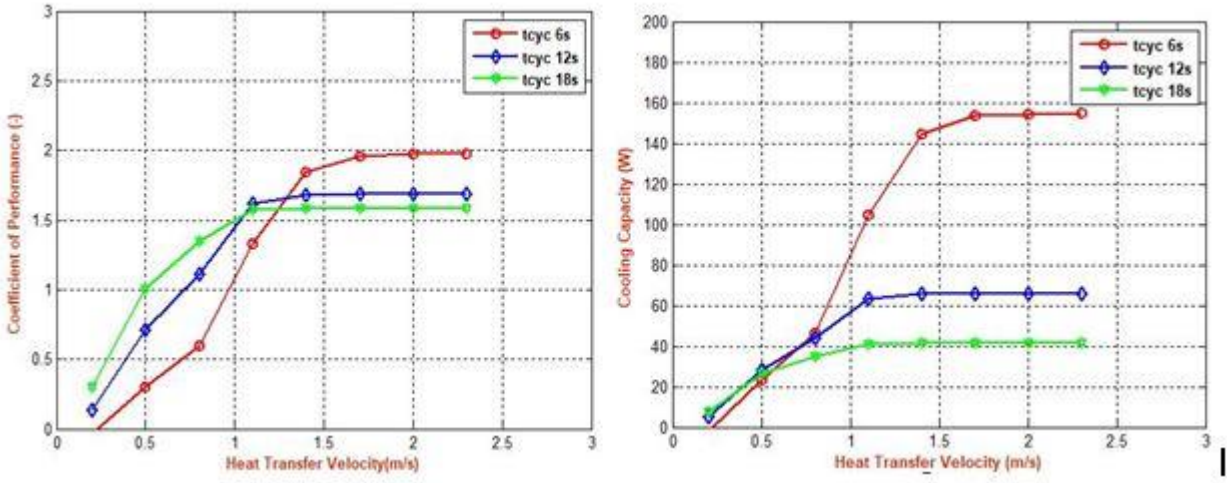

Fig 10:COP and cooling capacity as a function of cycle duration (Ni-Ti alloy, uHT = 1.2 m/s, L = 0.254 m, OD = 0.005 m, ID = 0.004 m, N = 19, ΔTlift = 10 K).

Fig. 10 shows significance of another important parameter to the performance, the flow rate (or corresponding velocity over the NiTi tube u_{HT}) during the heat transfer process.. A higher flow rate increases convective heat transfer coefficient, and so heat transfer effectiveness. With increase of u_{HT} improvement in COP is observed upto certain point only beyond that there is no significant improvement in COP. This is because the majority bottleneck limiting a higher effectiveness is the heat transfer duration rather than heat transfer flow rate at that point Optimum heat transfer velocity is found to be

1.2m/s. The second observation is that COP/ capacity curves have tiny oscillations at different flow rates rather than stay monotonically increasing to saturation values. This is due to the temperature oscillation transient effect during the heat transfer process when the thermal mass of fluid inside the heat source/heat sink is in the same magnitude as the NiTi bed fluid. The same figure also indicates that with a longer cycle duration, this transient effect reduces significantly.

iii) Effect of Heat recovery velocity u_{HR} on system COP and Cooling capacity:

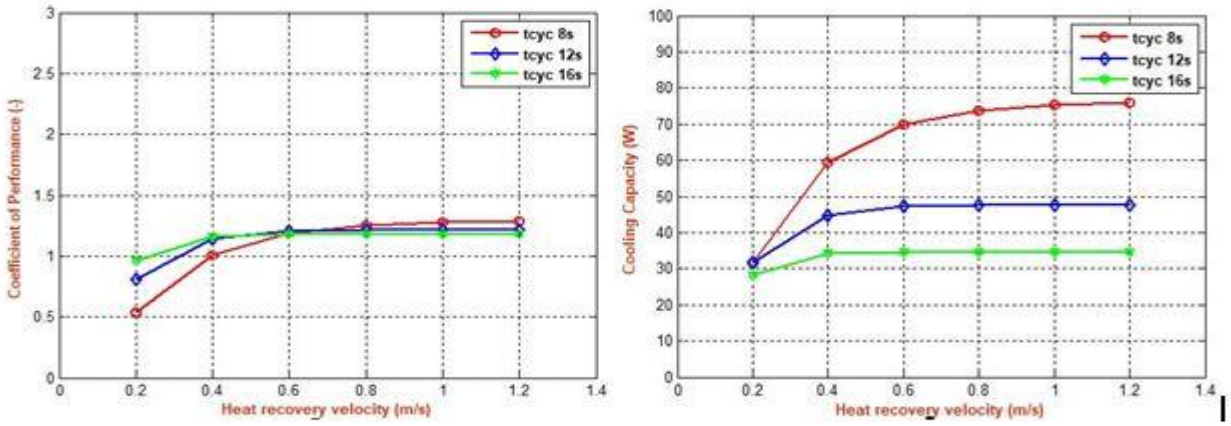

Fig 11:COP and cooling capacity as a function of heat recovery flow rate (Ni-Ti alloy, uHT = 1.2 m/s, L = 0.254 m, OD = 0.005 m, ID = 0.004 m, N = 19, ΔTlift = 10 K).

Heat recovery velocity means velocity of fluid in heat recovery loops. Fig 11 shows the variation system COP and Cooling capacity with heat recovery velocity. Slower heat recovery process is considered to be a more reversible design as a result heat recovery efficiency increases but requires a longer heat recovery duration, and therefore, left less time for heat transfer because of that heat transfer effectiveness decreases. By using the analytical COP in Eq. 10 again, the first effect is that a smaller u_{HR} returns a high recovery efficiency η, with a Side effect of smaller heat transfer effectiveness ε In fact, for the 12 s t_{cyc} case , η is improved from 0.15 to 0.46 when u_{HR} reduces from 1m s^{-1} 0.4 m s^{-1}, at a cost of losing ε from 0.95 to 0.87. Below 0.4 m s^{-1} threshold, even with higher η (upto 0.55), the system overall capacity or COP still reduces, since the effecivenss ε reduces dramatically from 0.87 to 0.52. These two major contradictory result in the existence of the optimum u_{HR} .Optimum heat recovery velocity is found to be 0.4m/s.

D) Effect of NiTi Tube Wall Thickness On System Performance:

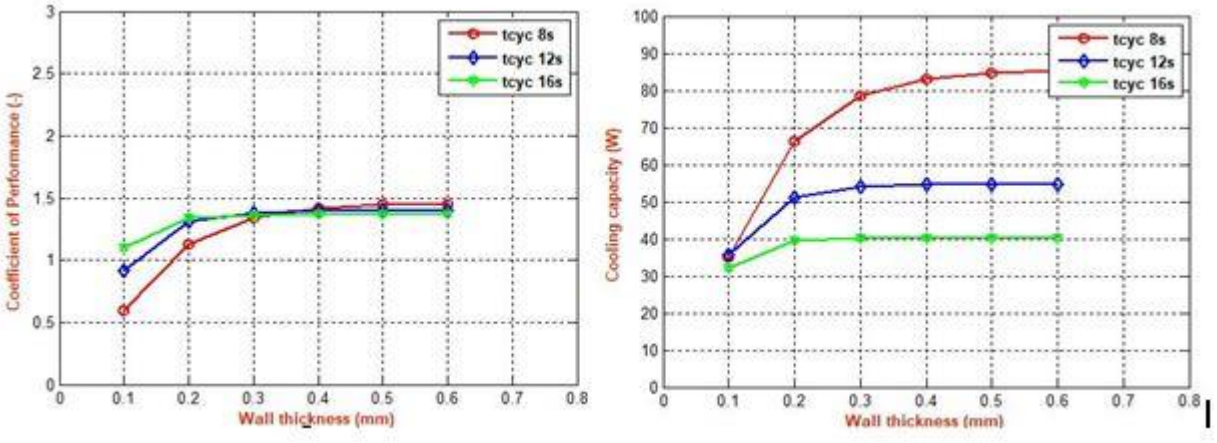

Fig 12:Effect of Ni-Ti tube wall thickness on COP and system cooling capacity (Ni-Ti alloy, uHT = 1.2 m/s, uHT = 0.2 m/s, L = 0.254 m, OD = 0.005 m, ΔTlift = 10 K, N = 13 – 19)

Unlike fluid refrigerants used in vapor compression systems, solid-state materials used in thermoelastic cooling have unique shapes and geometries. The geometries could significantly to the transient behaviour during the heat transfer and heat recovery process. Therefore, the effect of geometries was investigated while the overall NiTi volume is maintained constant to guarantee the same amount of material latent heat. NiTi tube's thermal mass does not allow high frequency

heat transfer, and thus it becomes a limiting factor to increase the cycle frequency. This issue can be resolved with the use of NiTi tubes with thinner walls. The NiTi tubes outside diameter (OD) remains constant while the wall thickness varies. However, the cooling capcity/ COP do not show an expected trend of increase as wall thickness decreases this is due to most of the cooling generated because of increased cycle frequency lost in heat transfer fluid loops.

E) Loss contributions:

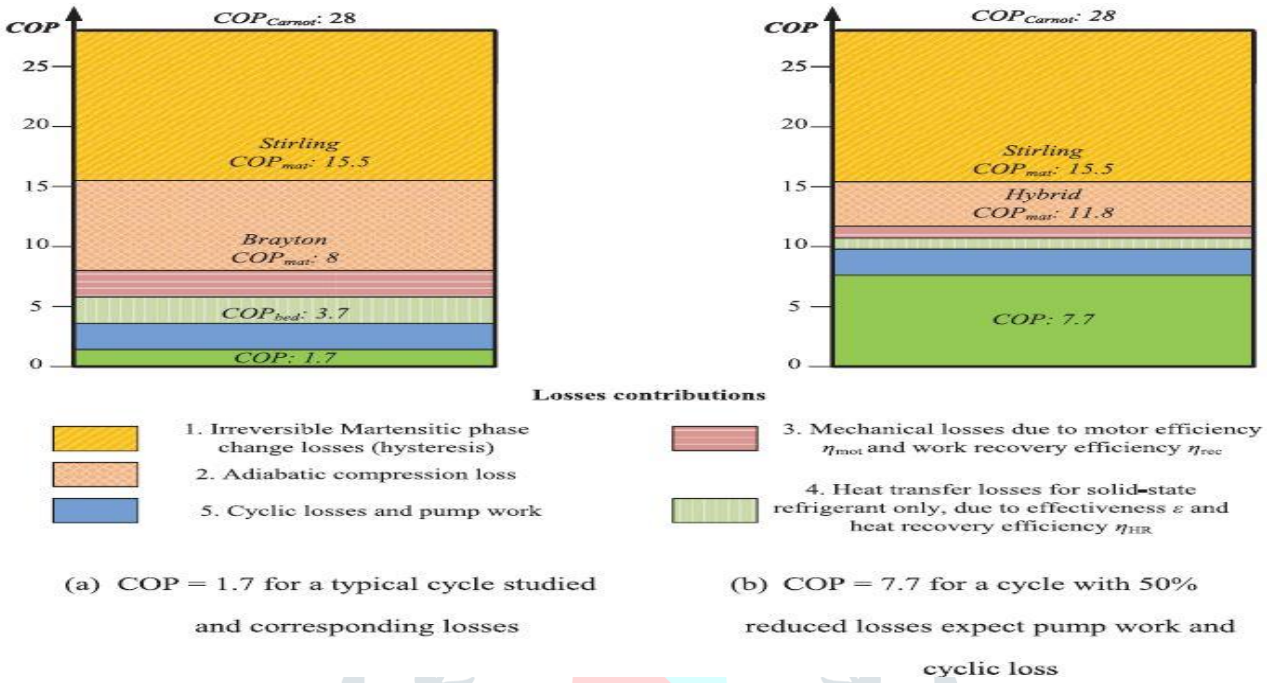

Fig. 13 Illustration of breakdown COP chart of the studied compressive thermoelastic cooling system

This session focuses on an overview of how the COP is varying with various losses. Fig. 13(a) is a stacked bar chart showing how the COP is degrading from Carnot COP to COP mat, and from material level all the way down to the system COP including the parasitic pump loss. The two COPmat are taken from Table 3-1 under isothermal and adiabatic compression, respectively. These two numbers could be boosted with other better alloys, as their mechanical properties and fatigue life are within tolerance. The first stage loss is due to material phase change irreversibility which is also measured by the material constant A(A-hysteresis loss constant) .Unlike liquid-vapor phase change in equilibrium, the solid-state phase change is highly irreversible contributed by "friction" interaction between different domains. The second stage loss is due to inefficiency of adiabatic compression, since the constant tempearature heat source/heat sink do not match with the variable temperature heat transfer process in a reverse Brayton cycle. The next stage loss is due to mechanical driving system inefficiency, which is also measured by the factor D defined in Eq. (5). When assuming a 90% motor efficiency, and 90% work recovery efficiency, we can get the D~.70. The fourth stage loss is due to heat recovery efficiency being less than 100%, which is shown in Eq. (9). The COP_{bed} equals 3.7 for a typical case simulation. The last stage loss is due to cyclic loss together with pumps parasitic power consumption. Factor F in Eq. (4) measures the cyclic loss, which is due to cyclic heating/cooling of fluid and corresponding pipe walls. If we consider heat transfer fluid pumps power consumption, assuming it to be equal to 20% of motor work, a system COP of 1.7 is achieved. This typical case evaluation is a starting point, since it is a random design without optimization. The previous parametric studies indicate that a lot of design and operating parameters do have optimum solution, therefore, it is possible to reduce the third and fourth stage losses through optimizing the operating and geometric parameters. It is also possible to use the hybrid cycle instead of the reverse Brayton cycle to improve the COPmat. With a conservative estimation with no improvement on cyclic loss and pump work consumption, a COP improvement estimation is then plotted on the right side of Fig.14, assuming first to fourth stage losses could be reduced to half compared to left side baseline scenario. The system COP is estimated to be 7.7 at 10 K lift under this estimation. A more conservative estimation could also be made, assuming the first stage loss remains the same since motor efficiency could not be improved significantly with a system COP of 5.2.

VII CONCLUSIONS

In this dissertation work the analytical and numerical model analysis of elastocaloric cooling systems is done. Two types of cycle design were demonstrated on the T-s and stress strain diagrams, applicable for both tensile driving mode and compressive driving mode. For the reverse Brayton cycle, the derived physics based analytical COP equation can be used as a simple calculation tool for future studies. The key parameters including the heat transfer effectiveness, the heat recovery efficiency, temperature lift and cyclic loss factor used in the analytical model can be derived from the developed dynamic model and influence of them on system COP is presented. Parametric studies indicated that for prototype development and improvement studies, the following parameters are important and should be optimized: cycle duration, heat recovery flow rate, SMA tube wall thickness and length. Among them, the cycle duration is most important. COP can be enhanced more than 30% by switching to a longer cycle duration, with a compromise of losing 37% cooling capacity. Therefore care should be taken while selecting cycle duration trade off should be made between improvement in system COP and loss in Cooling capacity. Optimum heat transfer velocity is found to be 1.2 m/s for better system COP and cooling capacity. Optimum heat recovery velocity is found to be 0.4 m/s for better system performance. High frequency heat transfer can be achieved with thinner NiTi wall tubes but the expected trend of increase in COP is not witnessed. NiTi tube length has less significance when compared to other parameters. Finally, the breakdown COPs of the reverse Brayton design compressive thermoelastic cooling system were discussed. A baseline system COP considering driving motor efficiency and necessary parasitic pump power consumption is 1.7, and an estimated system COP with improvement ranges from 5.2 to7.7, all evaluated under 10 K lift. Possible performance improvement methods include looking for more efficient SMA material, optimizing operating and geometric parameters, better design of heat transfer loops or use high efficient pumps, and more efficient design of mechanical driving systems. Overall, based on the modelling results from current study, this new cooling technology is promising but also challenging, and requires more research effort to demonstrate its potential in real prototype and optimize its performance.

REFERENCES

[1] S. Qian, D. Nasuta, A. Rhoads, Y. Wang, Y. Geng, Y. Hwang, R. Radermacher, I. Takeuchi. “Not-in-kind cooling technologies: a quantitative comparison of refrigerants and system performance”, Int. J. Refrig. 2015 (in-press)
[2] Otsuka, K., & Wayman, C. (1998). Shape Memory Materials. Cambridge, UK: Cambridge University Press
[3] Buehler, W., Gilfrich, J., & Wiley, R. (1963). Effect of low temperature phase 242 changes on the mechanical properties of alloys near composition TiNi. Journal of Applied Physics, 34, 1475-1477
[4] Romero, R., & Pelegrina, J. (2003). Change of entropy in the martensitic transformation and its dependence in Cu-based shape memory alloys. Materials Science and Engineering A, 354, 243-250
[5] Miura, S., Moruta, Y., & Nakanishi, N. (1975). Superelasticity and shape memory effect in Cu-Sn alloys. In J. Perkins, Shape Memory Effects in Alloys (pp. 389-405). New York, USA: Springer.
[6] Banks, R. (1975). USA Patent No. US3913326 A
[7] Johnson, A. (1977). USA Patent No. US4055955 A
[8] Hugenroth, J. (2002). USA Patent No. US6367281 B1
[9] Cui, J., Wu, Y., Muehlbauer, J., Hwang, Y., Radermacher, R., Fackler, S., . . . Takeuchi, I. (2012a). Demonstration of high efficiency elastocaloric cooling with large Delta T using NiTi wires. *Applied Physics Letters, 101*, 073904.
[10] S. Qian, J. Ling, Y. Hwang, R. Radermacher, I. Takeuchi. “Thermodynamic cycle analysis and numerical modeling of thermoelastic cooling systems”, Int. J. Refrig., 56, 65-80.
[11] www.wikipedia.org